Rare Metal Materials and Engineering
Volume 49, Issue 6, June 2020
Available online at www.rmme.ac.cn

Science Press

Cite this article as: Rare Metal Materials and Engineering, 2020, 49(6): 1840-1853.

ARTICLE

Flow Stress Prediction Model of 6061 Aluminum Alloy Sheet Based on GA-BP and PSO-BP Neural Networks

Ding Fengjuan[1], Jia Xiangdong[1], Hong Tengjiao[2], Xu Youlin[1]

[1] Nanjing Forestry University, Nanjing 210037, China; [2] Anhui Science and Technology University, Bengbu 233100, China

Abstract: Taking 6061-T6 aluminum alloy cold-rolled sheet as the research object, the plastic deformation behavior of 6061 aluminum alloy at different heat treatment temperatures (500, 530, 560 and 590 °C) was analyzed through uniaxial tensile test, metallographic test and microhardness test. Combined with experimental data and BP, GA-BP and PSO-BP neural networks, the constitutive models of this material under different heat treatment temperature conditions were constructed. The results show that BP, GA-BP and PSO-BP neural network models can better fit the flow behavior of 6061 aluminum alloy under different heat treatment temperature conditions, but PSO-BP neural network model has higher prediction accuracy and good performance in predicting the flow stress of 6061 aluminum alloy, and its average absolute error (MAE), average relative error (AARE) and the correlation coefficient (R^2) are 1.89, 1.56% and 0.9965, respectively.

Key words: 6061aluminum alloy; flow stress; artificial neural network; genetic algorithm; particle swarm optimization; heat treatment process

Aluminum alloy is one of the most commonly used materials in the fields of machinery, electronics, rail transit, aerospace, etc, due to its lightweight, high strength, and good formability[1]. Therefore, it is important to assess all fundamental properties of this material, including the mechanical feature of plastic deformation. The process of plastic deformation in metals under the effect of external strain factors is influenced by the non-linear relationship between strain rate, temperature, and flow stress. The development of a precise constitutive equation that can effectively correlate these properties and describe the plastic deformation behavior in materials has been a subject for many scientific researchers.

Abd El-Aty et al[2] and Wang et al[3] proposed a new constitutive equation of AA2060-T8 aluminum alloy and 7050-T7451 aluminum alloy, respectively, based on the Johnson-Cook model and the coupling of temperature, strain, and strain rate effects. Rasaee et al[4] also established a constitutive equation based on the Johnson-Cook model of Al2024, that accounts for the effects of hardening and softening behavior, as well as the correlation between different parameters. Xiang et al[5] investigated the high temperature deformation behavior of Al-Mg-Si-La alloy and the strain factor was included in the constitutive model based on the Arrhenius equation and Z parameter. Using this model, the relationship between the material constants (Q, ln$A$, n, and α) and true strain can be expressed by a 6th-order polynomial function, achieving accurate estimation of the flow stress in Al-Mg-Si-La alloy. Liu et al[6] proposed an improved Arrhenius-type constitutive model that well predicts the increase in flow stress of 2219 Al alloy with decreasing the temperature and/or increasing the strain rate. Haghdadi et al[7] established a constitutive model to calculate the flow stress of A356 aluminum alloy based on the Arrhenius-type equation and Zener-Hollomon parameter. Chamanfar[8] built a constitutive equation of a newly developed and homogenized AA6099 alloy, by which the relation between flow stress and deformation temperature and strain rate was derived based on a power-law empirical model, and it shows that the main flow

Received date: October 26, 2019
Foundation item: Natural Science Foundation of Jiangsu Higher Education Institutions of China (18KJB460020); High-level (Higher Education) Science Foundation of Nanjing Forestry University (GXL2018020); Youth Science and Technology Innovation Foundation of Nanjing Forestry University (CX2018027)
Corresponding author: Jia Xiangdong, Ph. D., Lecturer, College of Mechanical and Electronic Engineering, Nanjing Forestry University, Nanjing 210037, P. R. China, Tel: 0086-25-85427790, E-mail: Jiaxd.good@163.com

softening mechanism of the investigated alloy is dynamic recovery. Chen et al[9] developed a new constitutive model considering the coupling effects of strain, strain rate, and temperature. Comparison of this model with J-C, KHL, ERK, and KL models shows that the flow stress predictions of the proposed model exhibit greater agreement with the experimental results over a wide range of temperature and strain rate. Wang et al[10] developed three phenomenological models, based on Johnson-Cook (J-C), Fields-Backofen (F-B), and Arrhenius-type models, to predict flow stress behavior of spray-formed 7055 aluminum alloy during compression. Among the three models, the modified J-C and F-B models cannot predict the hot deformation behavior of 7055 aluminum alloy well due to the large deviation in line regression fitting, while the modified Arrhenius-type model yields the best results, as it combines the effects of strain rate and temperature. He et al[11] proposed a constitutive model that accounts for local strain rate evolution based on the Fields-Backofen (F-B) model and it was used to predict the flow stress behavior of 2024 aluminum alloy. Compared to the original F-B model, the predictions of proposed equation are more similar to the experimental results. Liu et al[12] established the constitutive model of homogeneous Al-Mg-Si-Mn-Cr alloy based on the modified J-C, Zerilli- Armstrong, and strain-compensated Arrhenius models. Among the three models, the strain-compensated Arrhenius model shows the best predictive accuracy, especially at low strain rates. Wang et al[13] used the Laasraoui-Jonas model, modified by introducing a term that accounts for flow softening induced by dynamic grain boundary migration, to predict the flow stress characteristics of Al-Mg-Si alloy. Li et al[14] developed a phenomenological constitutive model of AA2219 by considering the negative-to-positive SRS and the coupling effects of strain and temperature. Lin et al[15] proposed a constitutive model of Al-Zn-Mg-Cu alloy based on dislocation density using an iterative procedure to describe the flow behavior under time-variant deformation conditions.

The above-mentioned constitutive models mainly use mathematical methods to characterize the flow stress characteristics and deformation mechanism of materials in the process of plastic deformation. Complicated mathematical expressions are prone to errors in the process of calculation, such as long calculation time and inconvenient application. In order to improve the prediction accuracy of the constitutive model, it is necessary to modify the influencing factors of flow stress due to different processing parameters and deformation mechanism. Compared with the traditional constitutive equation, neural network theory is more mature. It has strong learning ability, generalization, fault tolerance and nonlinear mapping ability, and can approach any continuous function, and artificial neural network has been used in much research to establish the stress-strain constitutive model. Xu[16] and Sheikh[17] et al used BP algorithm to establish a constitutive relationship model of Q345 steel alloy and AA5083 aluminum alloy, respectively. The established models can predict the mechanical properties of the investigated alloys at different temperatures, as well as show the complex non-linear relationship between ultimate performance and heating temperature. Zhang[18] and Wan[19] et al developed the constitutive models of Al6181H18 and Ti-2.7Cu alloy, respectively, based on the BP and ATPSO-BP models. The flow stress characteristics of 7075, 6A02, and 5754 aluminum alloys were studied by Quan[20], Han [21], and Huang [22] et al, respectively, using isothermal compressive tests. For each material, a constitutive model was established based on the Arrhenius-type equation or BP algorithm. The obtained results show that the BP neural network model exhibits excellent predictive capability in the complex flow behavior of as-extruded 7075 aluminum alloy and thus has great potential in applications involving hot deformation processes. Similar to the 7075 aluminum alloy, the BP neural network model shows enhanced performance in terms of flow stress prediction for 6A02 alloy, compared to the Arrhenius-type model. Finally, the GA-BP neural network model yields the greatest predictive efficiency for the 5754 aluminum alloy throughout the entire deformation process.

Base on the above research, it is concluded that BP and optimized BP neural networks can be used to predict the complex flow behavior of metal materials in the process of plastic deformation. BP neural network is better than the traditional constitutive method in predicting performance, and can better characterize the non-linear mapping relationship between flow stress and deformation temperature, strain rate and strain. However, BP neural network has some inherent flaws, such as the need to learn a large number of sample data to ensure the prediction accuracy, the slow learning speed, and tendency of falling into local minimum value and network instability[23]. In addition, the initial weights and thresholds of randomly selected neurons have great influence on the stability and prediction accuracy of the network. Therefore, it is necessary to optimize the BP neural network to obtain a more accurate and reliable network model and better prediction performance. In this study, we assessed the flow stress properties of 6061 aluminum alloy, which is a thermally reinforced Al-Mg-Si alloy characterized by lightweight, high strength, good formability and has a wide range of applications. In order to study the effect of different heat treatment temperatures on the plasticity and flow behavior of the investigated alloy, the commercial 6061-T6 aluminum alloy sheet was used as the research object and the flow stress characteristics of 6061-T6 aluminum alloy after reheating at different heating temperatures were studied. In addition, the flow stress of 6061 aluminum alloy under various heat treatment conditions was theoretically predicted by constitutive models, which were developed based on BP, GA-BP and PSO-BP neural network models, and the prediction capability of

these three models was analyzed by statistical analysis methods.

1 Experiment

The elemental composition of the 6061-T6 aluminum alloy sheets used in this study was 1.3 wt% Si, 0.26 wt% Mg, 0.5 wt% Fe, 0.5 wt% Cu, 0.2 wt% Mn, 0.1 wt% Cr, 0.2 wt% Zn, 0.15 wt% Ti and balance Al. The original metallographic structure of 6061-T6 aluminum alloy is shown in Fig.1.

It can be seen from Fig.1, the 6061-T6 aluminum alloy has an obvious recrystallization process. Due to the elimination of the fiber structure caused by the rolling deformation of the plate, equiaxed crystals form with large individual size differences, and there are a large number of fine second phases inside the grains, with high dispersion degree. These dispersed second phases will increase the resistance of the dislocation motion of the crystal grains, leading to the increase of the strength and hardness of 6061 aluminum alloy and deterioration in plastic properties.

The existing research results show that the solidus and liquidus temperature of 6061 aluminum alloy are 582 and 652 °C[24,25], respectively, and the dynamic recrystallization phenomenon is obvious when the heating temperature is 300~500 °C [26]. Therefore, in order to obtain the influence of different heat treatment temperatures on the flow stress of 6061 aluminum alloy, a single variable control method was used in the research process. Under the same holding time and cooling mode, the van-type resistance heating furnace (SX2-4-10) was used to heat treat the aluminum alloy samples and the heating temperature was designed as 500, 530, 560 and 590 °C. Before uniaxial tensile tests, 6061-T6 aluminum alloy sheets were heat treated for 2 h in a van-type resistance heating furnace (SX2-4-10) according to the temperature plan displayed in Table 1.

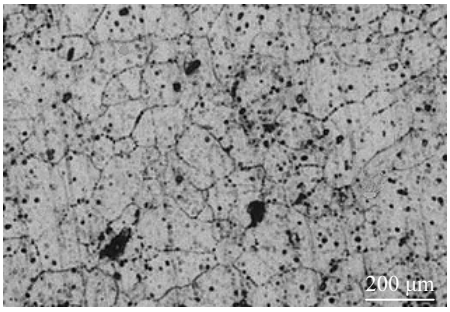

Fig.1 Original metallographic structure of 6061-T6 aluminum alloy

Table 1 Heat treatment of 6061-T6 aluminum alloy samples

Process No.	Heat treatment
1	500 °C for 2 h and air cooling
2	530 °C for 2 h and air cooling
3	560 °C for 2 h and air cooling
4	590 °C for 2 h and air cooling

The effects of different heat treatment temperatures on the flow stress and hardness of 6061 aluminum alloy were obtained by CMT5105 electronic universal testing machine and 4P2MVA Vickers hardness tester.

The microstructure of 6061 aluminum alloy at different heat treatment temperatures was observed by XJP-6A optical microscope. Before observation, 6061 sheet was cut into 5 mm×3 mm×1 mm metallographic samples by metal shears, and then the samples were cold mounted by acrylic powder and curing agent. 6061 aluminum alloy specimens were pre-ground with 800~2500 sandpaper and polished mechanically. Then chemical etching was carried out with Keller (1 mL HF+1.5 mL HCL+2.5 mL HNO_3+95 mL H_2O) reagent for 16~100 s, and then washed with alcohol and dried. Finally, the metallographic structures were compared and analyzed by metallographic microscope.

2 Results and Discussion

2.1 True stress-strain curves

The true stress-strain curves of 6061 aluminum alloy at different heat treatment temperatures were measured by uniaxial tensile test, as shown in Fig.2.

The experimental results shown in Fig.2 indicate that heating temperature during heat treatment, strain and strain rate during deformation have a great influence on the flow stress behavior of 6061 aluminum alloy. Within a specific temperature range, flow stress increases with increasing the strain rate, showing an obvious strain rate hardening effect. Under the same heat treatment and strain rate conditions, the flow stress of 6061 aluminum alloy increases with the increase of plastic strain, and the flow stress curves are relatively smooth during the initial tensile stage. However, as the plastic deformation increases, the subsequent flow stress curves have obvious serration. This indicates that, under uniaxial tensile conditions, the plastic deformation instability and PLC effect are caused by the interaction between dynamic strain aging and dislocation[27].

The yield stress curve, tensile strength curve and uniform elongation curve of 6061 aluminum alloy at different heat treatment temperatures are shown in Fig.3~5, respectively.

According to the variation curve of yield stress with heat treatment temperatures shown in Fig.3, it can be known that the yield stress of 6061-T6 aluminum alloy at room temperature is about 250 MPa, which is obviously higher than the yield stress of 6061 aluminum alloy at different heat treatment temperatures. At the same strain rate, the yield stress of the reheated 6061 aluminum alloy decreases sharply and then increases slowly with the increase of heat treatment temperature. When the heating temperature is increased from 500 °C to 590 °C, the yield stress of 6061 aluminum alloy is gradually increased during the stretching process. The change rule of tensile strength is similar to that of yield stress.

As shown in Fig.4, the tensile strength of 6061-T6 aluminum

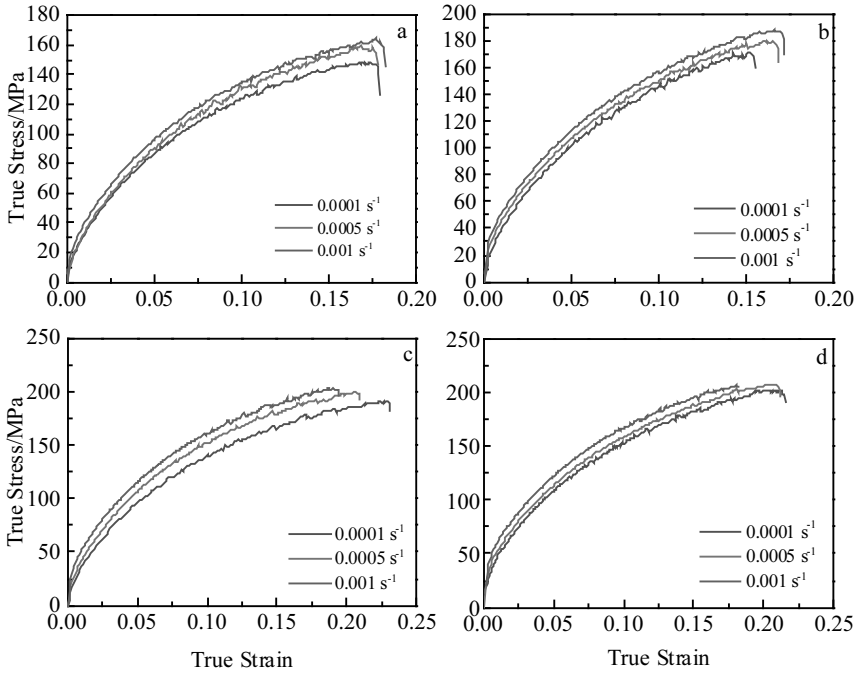

Fig.2 True stress-strain curves of 6061 aluminum alloy samples measured at different temperatures: (a) 500 °C, (b) 530 °C, (c) 560 °C, and (d) 590 °C

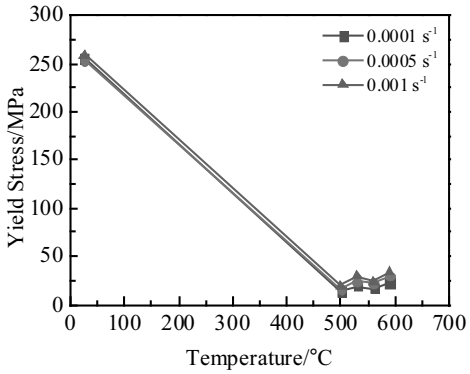

Fig.3 Yield stress curves of 6061 aluminum alloy at different heat treatment temperatures

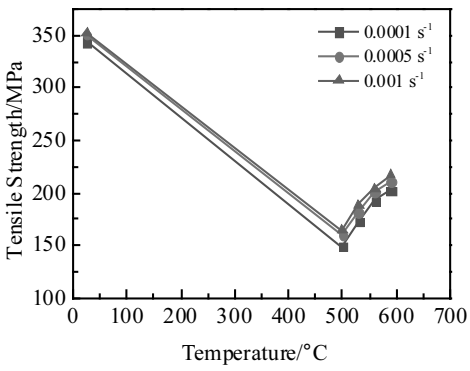

Fig.4 Tensile strength curves of 6061 aluminum alloy at different heat treatment temperatures

alloy at room temperature is about 350 MPa, which is significantly higher than that of 6061 aluminum alloy at different heat treatment temperatures. At the same tensile strain rate, the tensile strength of 6061 aluminum alloy decreases sharply and then increases rapidly with the increase of heat treatment temperature. Fig.5 shows the curve of uniform elongation changing with the heat treatment temperature. It can be seen from Fig.5 that the uniform elongation of 6061-T6 aluminum is very low at room temperature, about 10%. When the heat treatment temperature rises to 500 °C, the uniform elongation of 6061 aluminum alloy is rapidly increased. when the heating temperature is increased from 500 °C to 530 °C, the uniform elongation of 6061 aluminum alloy after heat treatment is remarkably lowered; when the temperature is increased from 530 °C to 560 °C, the uniform elongation of the heat treated 6061 aluminum alloy increases with the increase of the heat treatment temperature; when the temperature continues to increase to 590 °C, the uniform elongation is reduced obviously. The uniform elongation of this alloy shows an overall upward trend, and reaches the maximum value (22.92%) when temperature is 560 °C and strain rate is 0.0001 s^{-1}.

In order to further investigate the influence of heat treatment temperatures on the plasticity of 6061 aluminum alloy, the hardness of this alloy after heat treatment at different temperatures was analyzed. The transformation rule of Vickers hardness with heat treatment temperature is obtained through experiments, as shown in Fig.6.

According to the hardness test results of 6061 aluminum alloy, the Vickers hardness value of the original 6061-T6 sheet

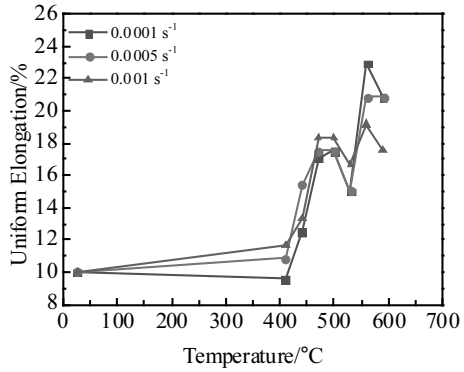

Fig.5 Uniform elongation curves of 6061 aluminum alloy at different heat treatment temperatures

selected for the test is 1325 MPa, and the hardness of the 6061 sheet obtained after reheating is significantly changed. As can be seen from Fig.6, when the heat treatment temperature rises to 500 °C, the hardness of 6061 aluminum alloy rapidly decreases from 1325 MPa to 575 MPa. However, when the heating temperature is higher than 500 °C, the hardness of the treated 6061 aluminum alloy increases, and the higher the heating temperature, the more obvious the increase in hardness. When the temperature is 590 °C, the maximum hardness is 937 MPa.

As can be seen from Fig.6, the hardness of 6061 aluminum alloy decreases first and then increases with the increase of heating temperature, and the hardness of 6061 aluminum alloy at test temperatures is lower than that of 6061-T6 aluminum alloy at the room temperature.

Through the above analysis, with the increase of heat treatment temperature, the mechanical properties of 6061 aluminum alloy are affected. The strength and hardness of this alloy are reduced, while the plasticity is optimized.

2.2 Microstructural evolution

Fig.7 is the microstructure of 6061 aluminum alloy sheet at different heat treatment temperatures; the holding time is 2 h and the cooling mode is air cooling. As can be seen from Fig.7, when the heat treatment temperature rises from 500 °C to 590 °C, the microstructures of 6061 aluminum alloy change obviously. Compared with the original microstructure of 6061-T6 in Fig.1 and reheated 6061-T6 aluminum alloy in Fig.7, when the heating

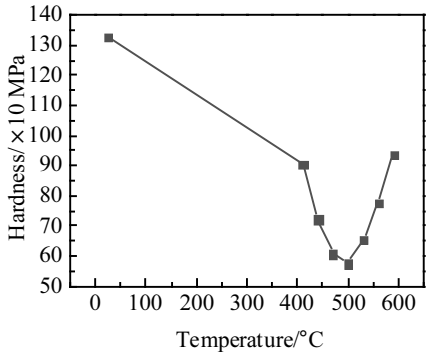

Fig.6 Vickers hardness curve of 6061 aluminum alloy at different heat treatment temperature

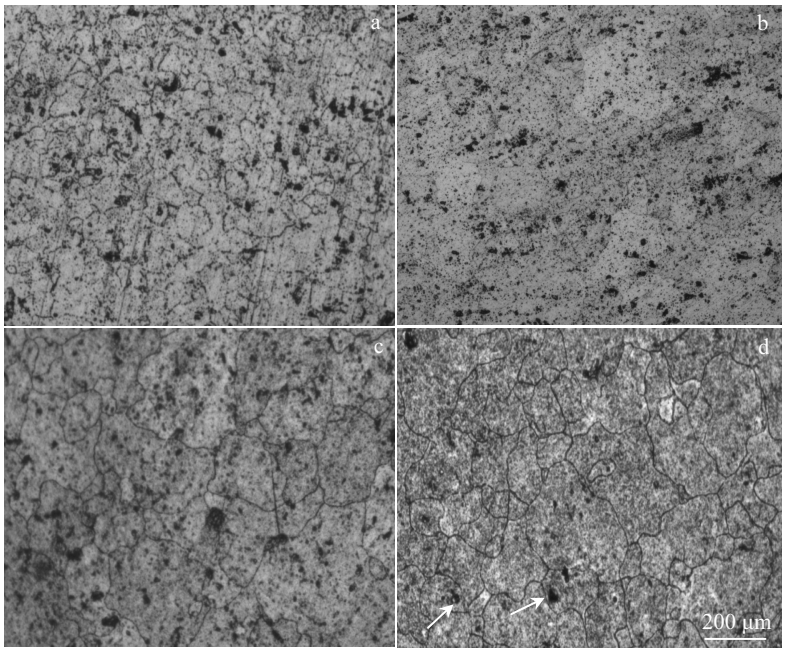

Fig.7 Metallographic structure of 6061 aluminum alloy at different temperatures: (a) 500 °C/2 h/AC, (b) 530 °C/2 h/AC, (c) 560 °C/2 h/AC, and (d) 590 °C/2 h/AC

temperature is 500 °C, recrystallization occurs inside the reheated aluminum alloy crystal, and the grain boundary is dissolved back, forming a crystal branch structure. As can be seen from Fig.7a, when the heating temperature is 500 °C, the recrystallized grains grow sufficiently and are distributed evenly. With the increase of heat treatment temperature, the driving force of recrystallization of 6061 aluminum alloy increases gradually, the degree of grain boundary connectivity is high, the second phase dissolves gradually, the second relative dislocation resistance decreases gradually, and the diffusion strengthening gradually disappears. Therefore, during the reheating process of 6061 aluminum alloy, when the heating temperature is up to 500 °C, the plasticity of the alloy is optimized, and the strength and hardness decrease significantly. When the heat treatment temperature continues to rise, it can be seen from the metallographic structure shown in Fig.7a and 7b that the crystal grains gradually grow up through the way of grain boundary merging, and the second phase begins to precipitate again in the grains. The strength and hardness of the alloy are improved, while the plasticity is declined. As can be seen from Fig.7c, when the temperature is 560 °C, the grains grow into continuous network by merging and the grain boundaries become clearer. The grain size of aluminum alloy grows obviously, and the degree of grain boundary connectivity is high. Due to the decomposition of supersaturated solid solution and the precipitation of fine second phase which plays a role of dispersion strengthening, the plasticity of the alloy is increased to the maximum (22.92%) and the strength and hardness are also significantly improved[28]. It can be seen from Fig.7d, when the heating temperature is 590 °C, a small amount of remelted balls appear in the aluminum alloy, and the structure pointed by the arrow is remelted balls. The grains of 6061 aluminum alloy are polygonal, and the grain boundaries are coarsened and clear. The strength and hardness of aluminum alloy increase due to the re-precipitation of the second phase and the formation of remelted ball, while the plasticity decreases slightly because of slight overheating.

Comparing the metallographic test results shown in Fig.1 and Fig.7 with the mechanical performance parameters shown in Fig.3~6, it can be seen that the metallographic analysis results are completely consistent with the mechanical property test results. Because of the obvious recrystallization process in the heat treatment of 6061 aluminum alloy, the properties of 6061 aluminum alloy heat treated at different temperatures are significantly different. The extent of recrystallization and the existence of the second phase are the main factors affecting the plasticity of 6061 aluminum alloy.

2.3 Constitutive model of 6061 aluminum alloy after heat treatment

As can be seen from the experiment results of the deformation law of the heat treated 6061 aluminum alloy in the stretching process, the flow stress of 6061 aluminum alloy after heat treatment is greatly affected by the heat treatment temperature, the strain rate and deformation during uniaxial stretching. It can be seen from the experimental data that there is a significant nonlinear relationship between the flow stress σ of 6061 aluminum alloy and heat treatment temperature T, strain rate $\dot{\varepsilon}$ and strain ε. Therefore, the establishment of a theoretical analysis model which can comprehensively reflect the influence of heat treatment temperature T, strain ε and strain rate $\dot{\varepsilon}$ on the flow stress σ is helpful to fully reveal the influence of heat treatment process parameters on the plastic properties of 6061 aluminum alloy.

2.3.1 BP artificial neural network model

The BP neural network is a multi-layer feed-forward neural network based on the error back-propagation algorithm. It usually consists of input, hidden, and output layers, and the topological structure is shown in Fig.8.

Compared with the traditional constitutive equation, the neural network theory is more mature. This network is characterized by a strong capacity for learning, generalization, fault tolerance, and non-linear mapping. It can approximate any continuous function and can be used to deal with non-linear problems such as material mechanical property prediction, flow behavior prediction and process parameter optimization[29,30]. It is mainly through the network training and learning of sample data to find out a certain rule, and use it to predict the output value of the input samples. In the training process of BP neural network, the threshold and weight of the neural network are adjusted continuously to make the output error of the network meet the requirements. Considering that the relationship between true stress σ of 6061 aluminum alloy, heat treatment temperature T, strain rate $\dot{\varepsilon}$, and strain ε is non-linear, the BP neural network algorithm may be used to develop a constitutive relation model that can accurately predict flow stress.

In order to accurately predict the flow stress of 6061 aluminum alloy after heat treatment, a three-layer BP neural network model was adopted. The heat treatment temperature T, strain rate $\dot{\varepsilon}$ and strain ε are taken as input variables, with the output variable as the true stress σ of 6061 aluminum alloy. There are 3 nodes in input layer and 1 in output layer for the constructed BP neural network, while the node number of implication layer is one of the key factors affecting the

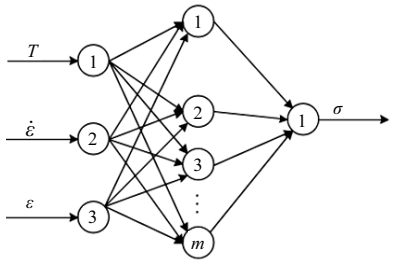

Fig.8 Structure of the BP neural network model

performance of BP neural network. If the number of hidden layer nodes is too many, the network training time will be increased, and over fitting will easily occur during the training. If the number of hidden layer nodes is less, the neuron training will be insufficient, and the expected goal of the network will not be achieved. In this study, the mean squared error value is taken as the goal, and the optimal number of implicit layer neurons is mainly obtained by trial and error. Through repeated training, when the number of hidden layer nodes is 7, the mean squared error is the smallest, and BP neural network prediction achieves the best performance. The expression of 3-layer BP neural network can be described as follows:

$$y_i = f(\text{net}_i) \tag{1}$$

where $\text{net}_i = \sum_{j=1}^{n} x_i \omega_{ij} - \theta$

where x_i is the input layer variables, representing the heat treatment temperature T, the strain rate $\dot{\varepsilon}$ and strain ε during uniaxial stretching; y_i is the output layer variable, that is, the flow stress σ of 6061 aluminum alloy, and ω_{ij} and θ are the weights and thresholds of neurons, respectively.

To achieve quick convergence and to avoid the saturation of neuron output, the experimental flow stress values obtained earlier are normalized using Eq.(2) so the data of model training samples should be within the range of [-1, 1]:

$$y = \frac{(y_{\max} - y_{\min})(x - x_{\min})}{x_{\max} - x_{\min}} + y_{\min} \tag{2}$$

x and y parameters in Eq.(2) represent the original data and normalized result, respectively, whereas $x_{\min}$ and $x_{\max}$ are the minimum and maximum values of the original data, respectively.

Three strain rates (0.0001, 0.0005, and 0.001 s^{-1}), four heating temperatures (500, 530, 560, and 590 °C), and the strain values (0~0.25) corresponding to the experimentally determined stress data were taken into consideration for the development of the BP neural network model of 6061 aluminum alloy. The total number of value sets is 408; 174 data values were extracted for model training, while the remaining values were used for model validation. The training goal of the BP neural network model was set to 10^{-7}, with learning rate, iteration number, and validation failure number parameters of 0.1, 1000, and 6, respectively.

2.3.2 GA-BP neural network model

The BP neural network is used to predict the flow stress of 6061 aluminum alloy under different heat treatment temperature conditions, which is easy to fall into the local minimum value, and the initial weight or threshold value of the neuron is taken randomly, which is easy to cause network oscillation and non convergence phenomenon, so a genetic algorithm is proposed to optimize the BP neural network and the reliability of the optimized BP neural network model is further verified. Genetic algorithm is a method to find the optimal solution through global search, which can effectively solve the problem of slow convergence and is easy to fall into local minimum of BP network. Its application for BP neural network model is mainly to optimize the initial weight and threshold of the network. In theory, the optimized BP neural network model achieves better prediction performance. Flow chart of BP network optimized by genetic algorithm is shown in Fig.9.

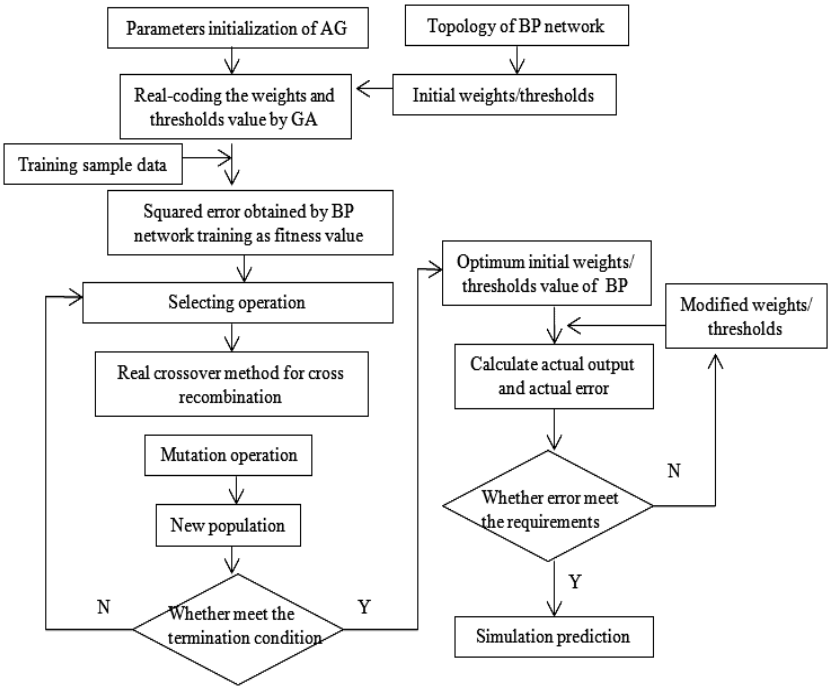

Fig.9 Flow chart of GA optimized BP neural network

In the genetic algorithm, the parameters of the genetic algorithm should be initialized first. In this model, the population size, the maximum number of iterations, the crossover probability and the mutation probability are set as 20, 10, 0.3 and 0.1, respectively. In order to improve the convergence speed and calculation accuracy of the genetic algorithm, the connection weight ω_{ij} and the threshold value θ of the BP neural network are encoded as a whole by real coding. According to the topological structure of BP neural network, the number of neurons in input layer, hidden layer and output layer is R, S_1 and S_2, respectively. Therefore, the chromosome length S in genetic algorithm can be expressed as follows:

$$S = RS_1 + S_1S_2 + S_1 + S_2 \tag{3}$$

After population initialization, according to the initial weight and threshold value of BP neural network, BP neural network is trained with sample set data. The squared sum of error between the output stress and expected output stress of BP neural network is used as individual fitness evaluation standard. The expression of fitness function F is as follows:

$$F = k(\sum_{i=1}^{n} | Y_i - O_i |) \tag{4}$$

where n, Y_i, O_i are expressed as the number of network output-layer nodes, the experimental stress value of the i-th node and the theoretical calculated stress value of the i-th node, respectively; k is the coefficient.

The roulette method is used to select the genetic algorithm, and the selection probability of each individual i is p_i.

$$p_i = \frac{J_i}{\sum_{j=1}^{N} f_j} \tag{5}$$
$$f_i = k / F_i$$

where F_i is the fitness value of individual i. Since the fitness value is as small as possible, the reciprocal of fitness is calculated before individual selection; k and n are the coefficient and the number of individual populations, respectively.

The real number crossing method is used for the cross operation. The cross operation method of the k-th chromosome a_k and the l-th chromosome a_l at j is as follows:

$$a_{kj} = a_{kj}(1-b) + a_{lj}b$$
$$a_{lj} = a_{lj}(1-b) + a_{kj}b \tag{6}$$

Mutation operation is selecting the j gene of the i-th individual a_{ij} for mutation, and the mutation operation method is as follows:

$$a_{ij} = a_{ij} + (a_{ij} - a_{\max}) f(g) \qquad r>0.5$$
$$a_{ij} = a_{ij} + (a_{\min} - a_{ij}) f(g) \qquad r\leqslant 0.5$$
$$f(g) = r_2(1 - \frac{g}{G_{\max}})^2 \tag{7}$$

where r_2 is a random number and g is the number of current iterations; $G_{\max}$ is the maximum number of evolution with a value of 10 and r is a random number between [0, 1].

In genetic algorithm, the optimal fitness corresponding individuals is obtained through selection, crossover and genetic operation, and the optimal weights and thresholds are given to the network for sample training and verification of network output.

2.3.3 PSO-BP neural network model

Particle swarm optimization (PSO) algorithm is similar to genetic algorithm. It is a kind of optimization algorithm based on iteration, but there is no cross, mutation and other operations. Compared with genetic algorithm, it has fewer parameters, simpler principle and easier implementation. Its search process is to constantly update its speed and position in the solution space through particles to follow the optimal particles. PSO algorithm can search the optimal threshold and weight of BP neural network in a large space, and to a certain extent, it avoids the traditional BP neural network using error back propagation to adjust the network connection weights, which is easy to fall into the problem of local optimal solution. In PSO algorithm, the connection weights of each layer of BP neural network are encoded into particles, and all particles form a group. The basic idea of particle swarm optimization is to find the optimal solution through cooperation and information sharing among individuals in a group. The flow chart of PSO-BP model is shown in Fig.10.

In N-dimensional search space, PSO algorithm first randomly initializes a population of particles, obtaining a position (Eq.8) and a random velocity (Eq.9) of the i-th particle. Then, fitness value F of each particle is determined based on Eq.(4).

$$X_i = (x_{i1}, x_{i2}, x_{i3}, x_{i4} ... x_{iN}) \tag{8}$$
$$v_i = (v_{i1}, v_{i2}, v_{i3}, v_{i4} ... v_{iN}) \tag{9}$$

For each particle, its fitness value is compared with the best position which has been obtained (i.e., pbest), and if it is better, then the pbest is replaced with the better one.

For each particle, its fitness value is compared with the best position which has been obtained in the group (i.e., gbest), and if it is better, then the gbest is replaced with the better one .

In each iteration, the optimal solution found by each particle is pbest, and the optimal solution found by the whole population is gbest. Each particle updates its speed and position through these two extremes. In the PSO, the velocity and position of each particle are updated by Eq.(10) and Eq.(11).

$$v_{\text{in}}^{k+1} = \omega v_{\text{in}}^{k+1} + c_1 r_1 (\text{pbest} - v_{\text{in}}^{k}) + c_2 r_2 (\text{gbest} - v_{\text{in}}^{k}) \tag{10}$$

$$x_{\text{in}}^{k+1} = x_{\text{in}}^{k} + v_{\text{in}}^{k+1} \tag{11}$$

where c_1 , c_2 is learning rate, r_1 , r_2 is random number from 0 to 1, ω is the inertia weight, and pbest is the best fitness value that has been obtained, gbest is the best fitness value which is obtained in the group.

Then, the optimal weights and thresholds computed by PSO

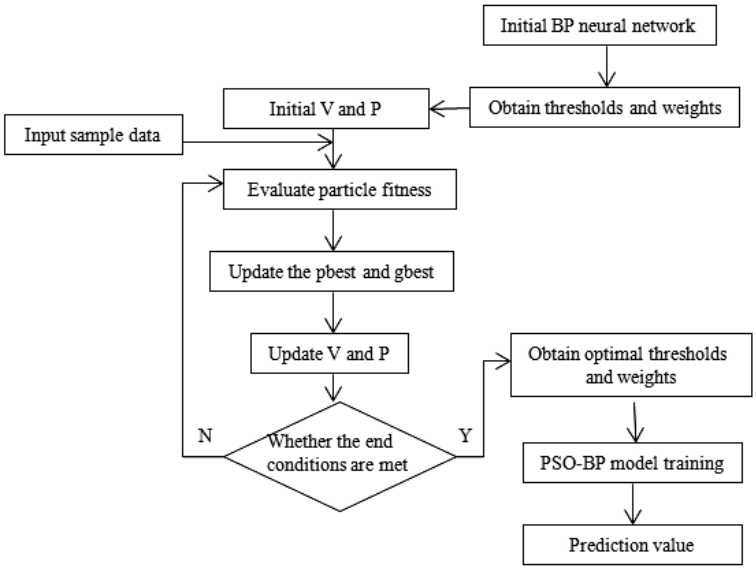

Fig.10 Flow chart of PSO optimized BP neural network

algorithm are given to the BP network for sample training and verification of network output.

In a sum, the PSO-BP neural network structure is 3-7-1. The necessary PSO parameters are set as follows: population size 30, evolutionary generation 50, number of particles 20, acceleration factor c_1=c_2=2; intervals of particle position and velocity are [-5, 5] and [-1, l], respectively.

2.3.4 Analysis and discussion

The performance index of the neural network is mainly assessed based on the value of mean squared error (MSE) between the actual output value and the expected output value of neural network. The smaller the MSE, the better the prediction performance of the network. In order to compare the performance indexes of the three training models of BP, GA-BP and PSO-BP neural networks, the mean squared error curves of the three training models are obtained through calculation, as shown in Fig.11. Fig.11a, 11b and 11c show the mean squared error curve of BP, GA-BP and PSO-BP neural networks, respectively.

From the mean squared error curve of the BP neural network shown in Fig.11a, the BP neural network was used to predict the flow stress of the heat treated 6061 aluminum alloy. After 33 iterations, the mean squared error of the test curve, validation curve and training curve converges to 0.000 482 47 approximately. From the mean squared error curve of the GA-BP neural network shown in Fig.11b, the mean squared error of the validation curve converges to 0.000 138 12 at epochs 25. However, the mean squared error of the validation curve and test curve is all greater than 10^{-4}. From the mean squared error curve of the PSO-BP neural network shown in Fig.11c, the mean squared error of the validation curve converges to 0.000 312 08 at epochs 86, while the mean squared error of the training curve converges to 10^{-4}. Comparing the mean squared error curves of BP, GA-BP and PSO-BP neural networks, it can be seen that GA-BP network is slightly better than BP and PSO-BP networks in predictive performance.

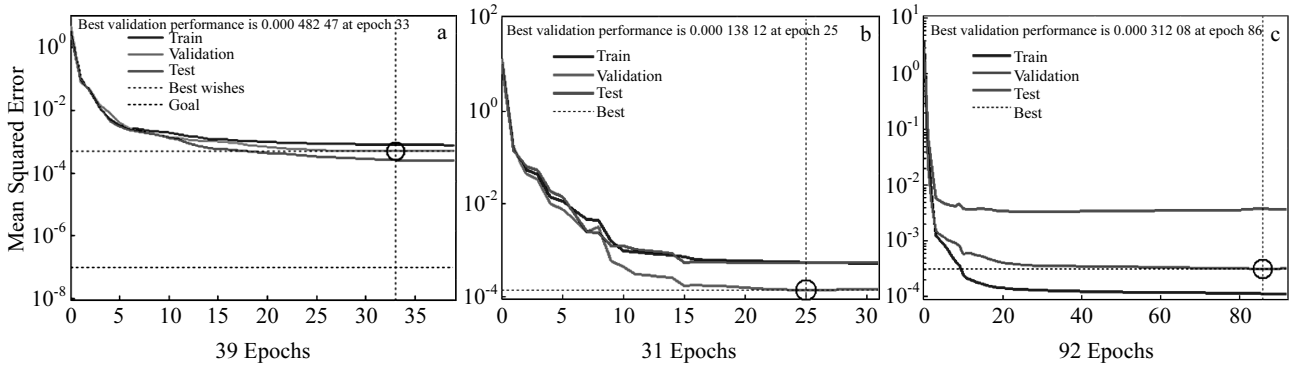

Fig.11 Mean squared error curves of neural network models: (a) BP, (b) GA-BP and (c) PSO-BP

In order to further verify the prediction performance of BP, GA-BP and PSO-BP neural network models for the flow stress of 6061 aluminum alloy after heat treatment, the stress fitting of training samples, verification samples, test samples and total samples by the three models is compared, as shown in Fig.12.

It can be seen from Fig.12a, BP neural network was used to predict the flow stress of 6061 aluminum alloy after heat treatment, and there is a large deviation between the output stress of a few validation samples and the experimental results. From Fig.12b, compared with experimental data, there is some deviation between the output stress of the training samples and test samples for GA-BP neural network model, which is consistent with the result shown in Fig.11b. From Fig.12c, the output stress of most test samples is greatly deviated from the experimental data, when PSO-BP neural network was used to predict the flow stress of 6061 aluminum alloy after heat treatment. The closer the *R* value to 1, the higher the degree of fitting of the neural network model. As can been from Fig.12, the fitting correlation coefficients of BP, GA-BP and PSO-BP neural network models are all higher than 0.994, which indicate that the training of the three models is sufficient. The trained neural network models have accurate prediction ability for the input samples.

In order to further verify the predicted performance of the trained BP, GA-BP and PSO-BP neural networks for the heat treated 6061 aluminum alloy, the output stress of the verification samples are compared with the experimental results, as shown in Fig.13 and Fig.14.

It can be seen from Fig.13 that the prediction value of BP, GA-BP and PSO-BP constitutive models is basically consistent with the experimental data, which demonstrates that BP, GA-BP and PSO-BP neural network models can accurately predict the complex flow behavior of 6061 aluminum alloy during the tensile process. However, there are errors in the prediction of the validation sample set using the three neural network models. Comparing the curves in Fig.13, it can be seen that the BP neural network has a relatively large error for the sample set number 210-217.

The flow stress values estimated using the trained BP, GA-BP and PSO-BP neural network models (symbols) are compared to the experimental data (lines), as shown in Fig.14.

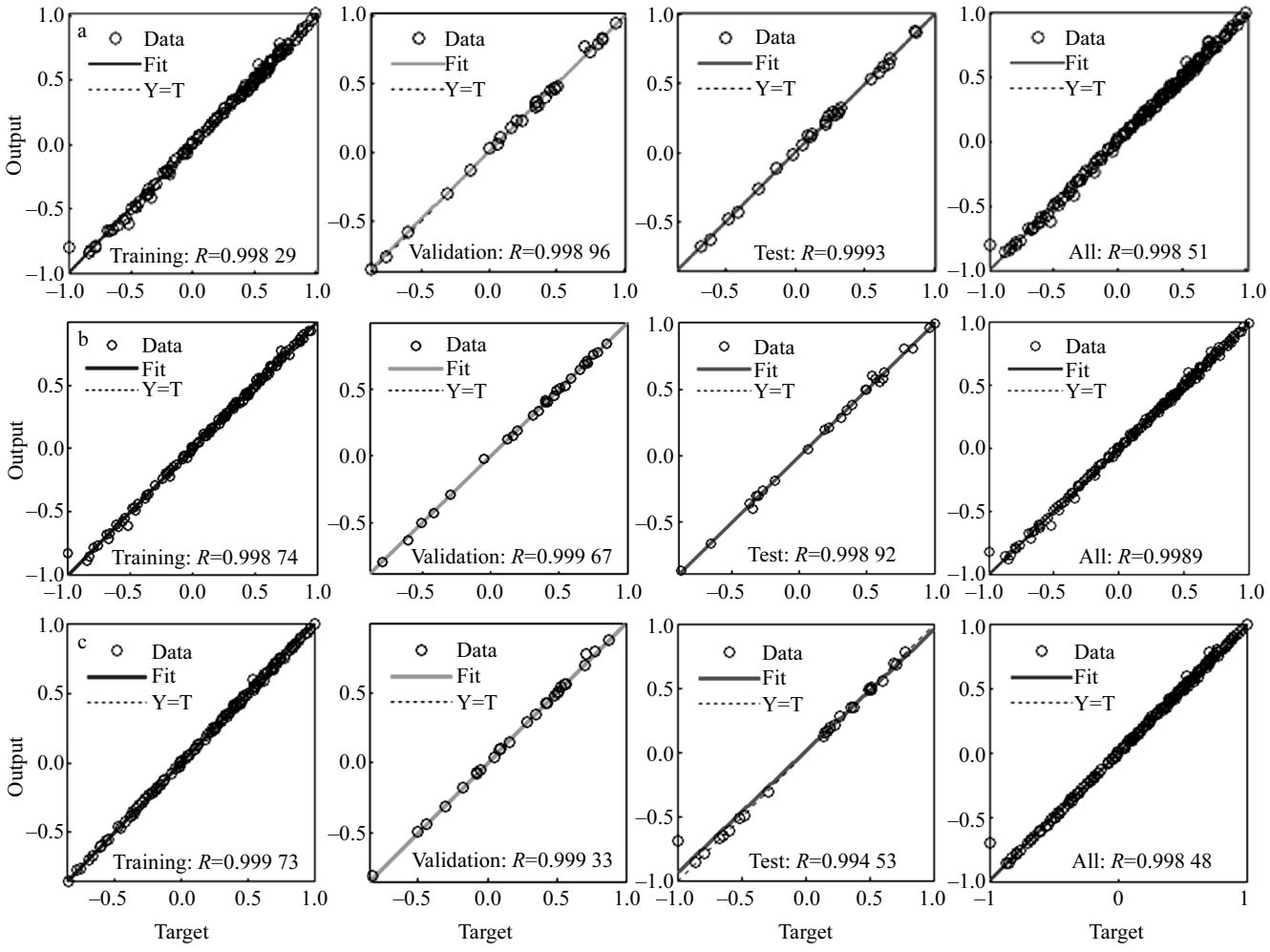

Fig.12 Fitting curves of neural network models: (a) BP, (b) GA-BP, and (c) PSO-BP

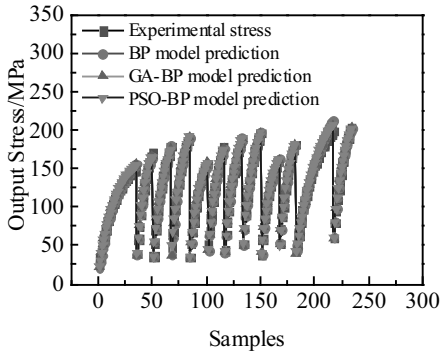

Fig.13 Validation results of neural network model

The comparison suggests that for all investigated strain rates and heat treatment temperatures, the flow stress of the heat treated 6061 aluminum alloy is calculated by PSO-BP neural network model, which is very well matched with the experimental values. As can be seen from the flow stress prediction curves shown in Fig.14a, when the heat treatment temperature is 500 °C and strain rate is 0.0001 s^{-1}, the prediction deviation of flow stress of 6061 aluminum alloy after heat treatment by BP neural network model is large, while that of GA-BP model is small. According to Fig.14c, when the heating temperature is 560 °C and strain rate is 0.001 s^{-1}, the prediction deviation of flow stress of 6061 aluminum alloy after heat treatment by BP model is large,

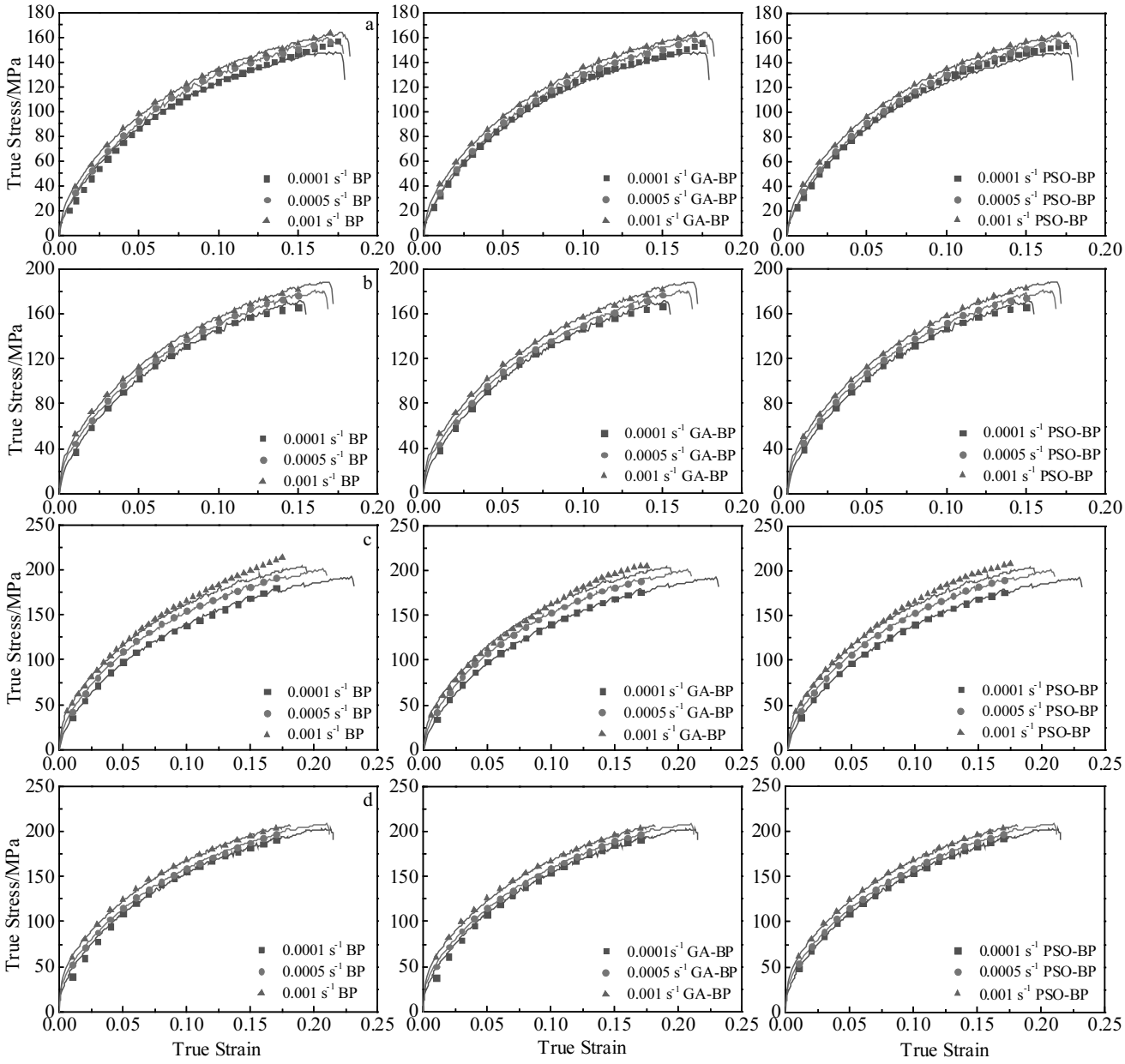

Fig.14 Comparison of the experimental and predicted results under different heat treatment temperature conditions: (a) 500 °C, (b) 530 °C, (c) 560 °C, and (d) 590 °C

while that of GA-BP model is small. From Fig.14b and 14d, when the heating temperature is 530 and 590 °C, the prediction results of flow stress of the heat treated 6061 by BP and GA-BP models are in good agreement with the experimental results. This shows that the initial weights and thresholds of BP neural network are optimized by genetic algorithm and particle swarm optimization algorithm, which can improved the prediction accuracy of BP algorithm.

The prediction error of neural network model indicates the accuracy of the model, so the prediction error and relative error of BP, GA-BP and PSO-BP neural networks are calculated by Eq.(12) and Eq.(13), as shown in Fig.15.

$$\text{Error} = E_i - P_i \tag{12}$$

$$\text{Relative error} = \frac{E_i - P_i}{E_i} \times 100\% \tag{13}$$

where E_i and P_i are the experimental result and the predicted result, respectively.

It can be seen from Fig.15 that the prediction error of BP neural network model varies from −15 MPa to 10 MPa, the relative error varies from −10% to 25%, and the number of samples with a large relative error is large; while the prediction error of GA-BP neural network model varies from −12.5 MPa to 10 MPa, and the relative error varies from −10% to 20%. The prediction error of PSO-BP neural network model varies from −12.5 to 10, and the relative error varies from −10% to 10%, and the number of samples with a large relative error is small. It is obvious that the prediction error of PSO-BP model is smaller and more accurate than that of the GA-BP model, and GA-BP model is more accurate than traditional BP model. This result is consistent with analysis of Fig.13 and Fig.14.

In order to further study the prediction error fluctuation of the flow stress of 6061 aluminum alloy after heat treatment by BP, GA-BP and PSO-BP neural network models, the error frequency histograms and fitting curve are drawn according to the prediction error of three neural network models, as shown in Fig.16.

From Fig.16, the results show that the absolute error of the GA-BP model and the PSO-BP model has a concentration near zero compared with that of the BP model. This phenomenon shows that the GA-BP and PSO-BP models have smaller errors and are more controllable than the traditional BP model.

The deviation between the predicted flow stress of 6061 aluminum alloy after heat treatment by BP, GA-BP and PSO-BP models and the experimental stress was compared as a whole. The correlation coefficient R^2 (Eq.(14)), average relative error AARE (Eq.(15))[31] and MAE (Eq.(16))[32] are used to measure the accuracy of the three prediction models. Comparison results of BP, GA-BP and PSO-BP models are shown in Fig.17 and Table 2.

$$R = \frac{\sum_{i=1}^{n}(E_i - \overline{E})(P_i - \overline{P})}{\sqrt{\sum_{i=1}^{n}(E_i - \overline{E})^2 (P_i - \overline{P})^2}} \tag{14}$$

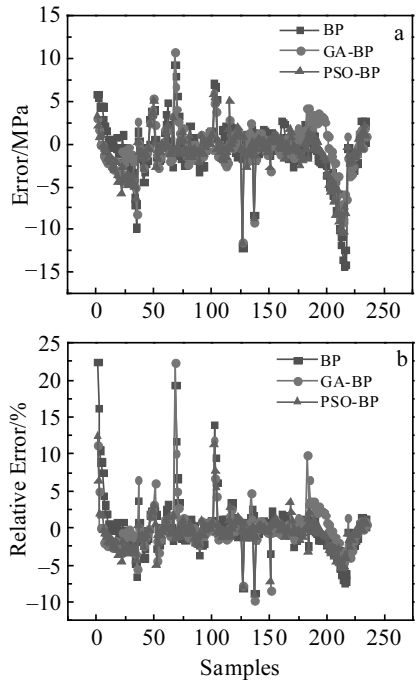

Fig.15 Prediction error (a) and relative error (b) of neural network models

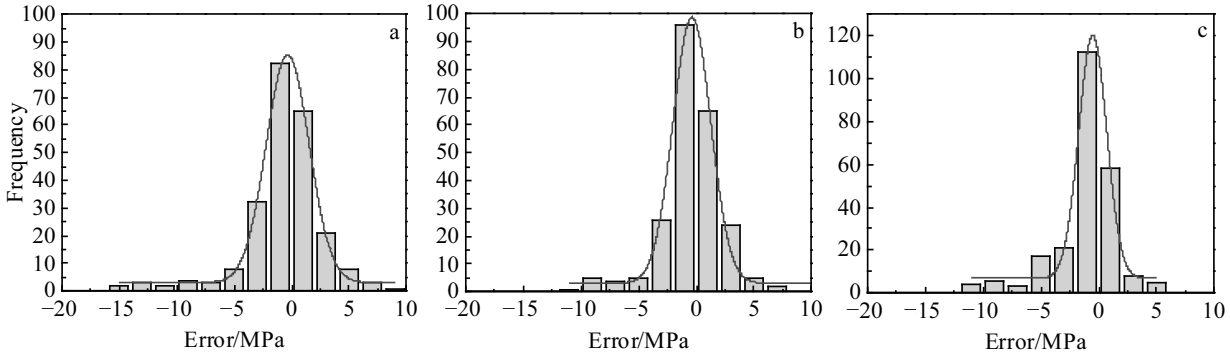

Fig.16 Error frequency histograms of 234 validation samples: (a) BP, (b) GA-BP, and (c) PSO-BP

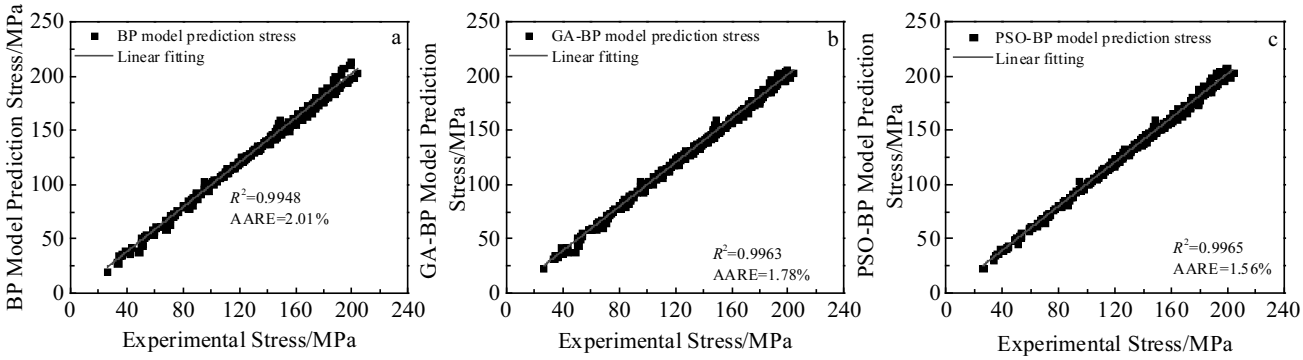

Fig.17 Correlation between experimental and predicted stress values: (a) BP, (b) GA-BP, and (c) PSO-BP

Table 2 Comparison of predicted performance of neural network models

Model	Performance		
	MAE	AARE/%	R^2
BP	2.226	2.01	0.9948
GA-BP	1.91	1.78	0.9963
PSO-BP	1.89	1.56	0.9965

$$\mathrm{AARE}=\frac{1}{N}\sum_{i=1}^{N}\left|\frac{E_i-P_i}{E_i}\right|\times 100\% \quad (15)$$

$$\mathrm{MAE}=\frac{1}{N}\sum_{i=1}^{N}|E_i-P_i| \quad (16)$$

where E and P are the experimental and predicted stress values, respectively; $\overline{E}$ and $\overline{P}$ are the average values of E and P, respectively; and N is the number of test data points.

Compared to the BP neural network model: firstly, mean absolute error (MAE) of the prediction value of PSO-BP model is 1.89, excelling BP model's 2.226 with 15% decline, which shows a smaller dispersion degree; then, the AARE of the prediction value of PSO-BP model is 1.56%, far more smaller than BP's 2.01%, which indicates a smaller difference between the prediction values and experimental values; finally, the correlation coefficients (R^2) in Fig.17a and 17c reflect that PSO-BP model's predicted results agree well with the experimental results (0.9965). In general, based on the performance indicators, PSO-BP model presents better performance than BP network model.

Compared to GA-BP model: firstly, MAE of the prediction value of GA-BP model is 1.91, while that of PSO-BP model is reduced by 1%, which shows a smaller dispersion degree; then, the AARE of the prediction value of PSO-BP model is decreased by 12.3%, which indicates a smaller difference between the prediction values and experimental values; finally, the correlation coefficients (R^2) of PSO-BP and GA-BP models in Fig.17b and Fig.17c reflect that both the predicted results of the two models agree well with the experimental data. In a sum, based on the above performance indicators, PSO-BP model is more accurate than GA-BP network model.

3 Conclusions

1) Under the same heat treatment conditions, the flow stress of 6061 aluminum alloy increases with the increase of tensile strain rate, and has obvious strain rate sensitivity.

2) The yield stress and tensile strength of 6061 aluminum alloy decrease sharply and then increase with the increase of heat treatment temperature. With the increase of heat treatment temperature from 500 °C to 590 °C, the plasticity of this alloy decreases first and then increases. When the temperature is 560 °C and strain rate is 0.0001 s^{-1}, the plasticity of 6061 aluminum alloy reaches its maximum value (22.92%). While the hardness of 6061 aluminum alloy decreases first and then increases with the increase of heat treatment temperature. The change rule of plastic properties and flow behavior of 6061 aluminum alloy with the increase of heat treatment temperature is the common result of recrystallization and dynamic strain aging.

3) BP, GA-BP and PSO-BP neural network models can better fit the flow behavior of 6061 aluminum alloy at different heat treatment temperatures, and PSO-BP neural network model has higher prediction accuracy and performs well in predicting the flow stress of 6061 aluminum alloy, whose average absolute error (MAE), average relative error (AARE) and the correlation coefficient (R^2) are 1.89, 1.56% and 0.9965, respectively.

References

1 Naronikar Aditya H, Jamadagni Akshay H N, Simha Amruthamshu *et al*. *International Conference on Advances in Materials and Manufacturing Applications (IConAMMA)*[C]. Bengaluru: IConAMMA, 2017

2 Abd El-Aty Ali, Xu Yong, Zhang Shihong. *Journal of Advanced Research*[J], 2019, 18: 19

3 Wang Bing, Liu Zhanqiang, Song Qinghua *et al*. *Journal of Manufacturing Science and Engineering*[J], 2019, 141(1): 1576

4 Rasaee S, Mirzaei A H. *Transactions of the Indian Institute of*

Metals[J], 2019, 72(4): 1023
5 Xiang Yanling, Xiao Sufen, Tang Zhenghua *et al*. *Materials Research Express*[J], 2019, 6(6): 1023
6 Liu Lei, Wu Yunxin, Gong Hai *et al*. *Transactions of Nonferrous Metals Society of China*[J], 2019, 29(3): 448
7 Haghdadi N, Zarei-Hanzaki A, Abedi H R. *Materials Science and Engineering A*[J], 2012, 535: 252
8 Chamanfar Ahmad, Alamoudi Mohammed T, Nanninga Nicholas E *et al*. *Materials Science And Engineering A*[J], 2019, 743: 684
9 Chen Guang, Lu Lianpeng, Ren Chengzu *et al*. *Journal of Alloys and Compounds*[J], 2018, 765: 569
10 Wang Xiangdong , Pan Qinglin, Xiong Shangwu *et al*. *Transactions of Nonferrous Metals Society of China*[J], 2018, 28(8): 1484
11 He Zhubin, Wang Zhibiao, Lin Yanli *et al*. *Metals*[J], 2019, 9(2): 243
12 Liu Shuhui, Pan Qinglin, Li Hang *et al*. *Journal of Materials Science*[J], 2019, 54(5): 4366
13 Wang Guan, Kou Linyuan, Liu Zhiwen *et al*. *Materials Research Express*[J], 2019, 6(5): 56 555
14 Li Z X, Zhan M, Fan X G *et al*. *Journal of Materials Engineering and Performance*[J], 2019, 28(1): 404
15 Lin Y C, Dong Wenyong, Zhou Mi *et al*. *Materials Science and Engineering A*[J], 2018, 718: 165
16 Xu Gening, Xu Ning, Liu Ying. *International Conference on Materials Processing and Mechanical Manufacturing Engineering*[C]. Changsha: MPMME, 2015
17 Sheikh H, Serajzadeh S. *Journal of Materials Processing Technology*[J], 2008, 196(1-3): 115
18 Zhang Jianping, Gao Pengfei, Fang Fang. *Computational Materials Science*[J], 2019, 163: 262
19 Wan Peng, Wang Kelu, Lu Shiqiang *et al*. *Journal of Engineering*[J], 2019, 47(4): 113 (in Chinese)
20 Quan Guozheng, Zou Zhenyu, Wang Tong *et al*. *Materials and Processes*[J], 2017, 36(1): 1
21 Han Ying, Yan Shun, Sun Yu *et al*. *Metals*[J], 2017, 7(4): 114
22 Huang Changqing, Jia Xiaodong, Hang Zhiwu *et al*. *Materials*[J], 2018, 11(5): 855
23 Wang Yujia, Wang Kelu, Lu Shiqiang *et al*. *Rare Metal Materials and Engineering*[J], 2018, 47(7): 2225 (in Chinese)
24 Tang Xiaoling, Shang Shuzhen, Lu Guimin *et al*. *Journal of Plasticity Engineering*[J], 2011, 18(1): 110 (in Chinese)
25 Liu Xinggang, Wang Guojun, Chen Lei *et al*. *Transactions of Materials and Heat Treatment*[J], 2016, 37(7): 77 (in Chinese)
26 Chen Xuejiao, Wang Huawei, Zhao Zhuo. *Steel Rolling*[J], 2019, 6(4): 7 (in Chinese)
27 Gupta S, Beaudoin A J, Chevy J. *Materials Science and Engineering A*[J], 2017, 683: 143
28 Liu F, Yu F, Zhao D *et al*. *Materials Science and Engineering A*[J], 2011, 528: 3786
29 Hülya D, Erdoğan Ö, Cevde M. *Mater Design*[J], 2006, 27(2): 156
30 Lin Y, Zheng Z Q, Zhang H F *et al*. *Trans Nonferrous Me*t[J], 2013, 23: 1728
31 Chen Can, Chen Minghe, Xie Lansheng *et al*. *Rare Metal Materials and Engineering*[J], 2019, 48(3): 827 (in Chinese)
32 Yun Deng, Xiao Hanjie, Xu Jianxin *et al*. *Saudi Journal of Biological Sciences*[J], 2019, 26: 1154

基于 GA-BP 和 PSO-BP 神经网络的 6061 铝合金板材流变应力预测模型

丁凤娟[1]，贾向东[1]，洪腾蛟[2]，徐幼林[1]
(1. 南京林业大学，江苏 南京 210037)
(2. 安徽科技学院，安徽 蚌埠 233100)

摘 要：6061 铝合金作为一种热可强化铝合金，具有良好的成形性能，但是其塑性流变应力受最终热处理工艺的加热温度、保温时间和冷却方式等参数的影响很大。因此，为了获得最终热处理工艺参数对 6061 铝合金板材的塑性性能及流变行为的影响，试验中以 6061-T6 铝合金板材为研究对象，通过单向拉伸试验、金相实验和硬度测试等方法研究不同热处理工艺参数(加热温度为 500、530、560 和 590 ℃、保温时间 2 h、冷却方式为空冷)对 6061 铝合金塑性性能和硬度的影响。通过单向拉伸试验获取不同热处理工艺参数条件下 6061 铝合金的真实应力-应变曲线；借助 BP、GA-BP 和 PSO-BP 神经网络构建不同热处理温度条件下 6061 铝合金的本构关系模型。结果表明，BP、GA-BP 和 PSO-BP 神经网络模型均能较好的拟合不同热处理温度条件下 6061 铝合金的流变行为，但是 PSO-BP 神经网络模型对 6061 铝合金流变应力的预测精度更高，模型预测性能更优越，其平均绝对误差(MAE)，平均相对误差(AARE)和相关系数(R^2)分别为 1.89，1.56%和 0.9965。

关键词：6061 铝合金；流变应力；人工神经网络；遗传算法；粒子群优化；热处理工艺

作者简介：丁凤娟，女，1988 年生，博士生，南京林业大学机械电子工程学院，南京 江苏 210037，E-mail: dingfengjuan2018@ 163.com